Magnesia–Incorporated Mesoporous Alumina with Crystalline Frameworks: A Solid Strong Base Derived from Direct Synthesis

ARTICLE *in* THE JOURNAL OF PHYSICAL CHEMISTRY C · OCTOBER 2009

Impact Factor: 4.77 · DOI: 10.1021/jp907224f

3 AUTHORS, INCLUDING:

Lin-Bing Sun
Nanjing Tech University
72 PUBLICATIONS **1,535** CITATIONS
SEE PROFILE

Xiao-Qin Liu
Harbin Medical University
39 PUBLICATIONS **433** CITATIONS
SEE PROFILE

Magnesia-Incorporated Mesoporous Alumina with Crystalline Frameworks: A Solid Strong Base Derived from Direct Synthesis

Lin-Bing Sun,* Wen-Hang Tian, and Xiao-Qin Liu

State Key Laboratory of Materials-Oriented Chemical Engineering, College of Chemistry and Chemical Engineering, Nanjing University of Technology, Nanjing 210009, China

Received: July 28, 2009; Revised Manuscript Received: September 18, 2009

By use of a surfactant templating method, the direct synthesis of magnesia-incorporated mesoporous alumina (*m*MgAl-γ) was realized via self-assembly of inexpensive inorganic salts. The structural and basic properties of the obtained materials were well characterized by various approaches. The results show that *m*MgAl-γ samples possess strong basicity with excellent water-resistant ability, well-defined mesoporous structure, and γ-Al_2O_3 crystalline frameworks. In comparison with wet impregnation that leads to structural damage, the direct synthesis strategy allows the mesoporous alumina to maintain good mesostructure. For example, the Brunauer−Emmett−Teller surface area of sample *m*MgAl(0.1)-γ can reach 328 $m^2 \cdot g^{-1}$, which is obviously higher than that of the sample prepared by a conventional impregnation method (239 $m^2 \cdot g^{-1}$). Further investigations evidence that the fabrication of suitable preassembled mesoporous precursors is crucial for the efficiency of the present direct synthesis strategy. In the process of calcination, the strongly basic species MgO was produced simultaneously and in situ coated on newly formed mesoporous γ-Al_2O_3 from preassembled precursors. Besides *m*MgAl-γ, mesoporous γ-Al_2O_3 materials functionalized with iron, chromium, and lead oxides were also successfully prepared, which demonstrates the generality of the strategy.

Introduction

Solid strong bases are extremely desirable for application in environmentally benign and economical chemical processes, since they can catalyze diverse reactions under mild conditions and minimize waste production.[1–3] So far various materials have been attempted as hosts for the preparation of solid bases. Due to their ordered microporous structure, zeolites can recognize, discriminate, and organize molecules precisely.[4,5] Considerable attention has been paid to the synthesis of basic materials derived from zeolites.[6–11] Nevertheless, the application of zeolites is limited by slow diffusion of substrates into their micropores for bulky molecular reactions and rapid deactivation owing to coke formation.[12]

Since the discovery of mesoporous silicas M41S, a series of mesoporous materials with various pore symmetries (e.g., hexagonal, cubic, lamellar, and wormhole) have been synthesized by the surfactant templating method.[13–18] These mesoporous silicas have larger pore openings and higher surface areas as compared with zeolites and are of great interest for adsorption, sensing, and catalysis.[19–23] As a logical remedy, the use of mesoporous silicas as hosts for the preparation of solid bases is expected. Many efforts have been dedicated to generating strong basicity on mesoporous silicas. Grafting organic bases at the silanol groups provided an interesting approach to create basic sites on mesoporous silicas;[24–26] however, the preparation of these organic−inorganic hybrid materials was complicated and expensive. Additionally, they can only be applied at temperatures lower than 170 °C due to the degradation of organic molecules at higher temperatures.[27] By treatment of mesoporous silicas such as MCM-41 and SBA-15 with gaseous NH_3, the oxygen in their frameworks can be partially displaced by nitrogen or NH_x species.[28,29] The oxynitride frameworks were thus formed and a new type of solid bases with mesostructure was produced. Nevertheless, the treatment temperature was usually higher than 900 °C and the basicity of the obtained materials was relatively weak. To improve the basicity, alkaline metal oxides were employed to modify mesoporous silicas. Mesoporous solid strong bases can be prepared by impregnation of MCM-41 with cesium acetate solution and subsequent calcination.[30] However, the obtained bases exhibited poor thermal and chemical stability since cesium oxide can react with silica and damage the framework of host.[31] Neutral salt KNO_3 has been widely used as the guest to generate strongly basic sites on various hosts.[32,33] Aiming at forming strong basicity on mesoporous silicas, SBA-15 was employed as host to disperse guest KNO_3. Unfortunately, the obtained material exhibited weak basicity and the mesostructure of SBA-15 was destroyed completely during the activation to decompose supported KNO_3.[34,35] Due to the reaction of strongly basic species with silica, it is difficult to generate strong basicity on mesoporous silicas. Up to now, the preparation of mesoporous strong bases remains a challenge.

Different from silica, alumina is a well-known host for many solid strong bases.[1,32] The reaction of strongly basic species with the host that occurred in silica-supported materials is absent. The successful synthesis of mesoporous alumina thus provides a good opportunity to prepare mesoporous strongly basic materials.[36,37] Unfortunately, two factors hinder the application of mesoporous alumina in preparing solid strong bases. The first factor is that the stability of mesoporous alumina is relatively poor, and structural damage occurs to a greater or lesser extent even if postsynthesis modification is performed carefully.[38] The second factor is that the frameworks of most mesoporous aluminas are amorphous, lacking the vacancies and active sites required for use as catalysts and catalyst supports.[39,40] These shortcomings also obstruct the application of mesoporous aluminas in preparing functional materials other than solid bases.

* To whom correspondence should be addressed: telephone +86-25-83587177; fax +86-25-83587191; e-mail lbsun@njut.edu.cn.

10.1021/jp907224f CCC: $40.75
Published on Web 10/13/2009

Therefore, the development of a novel synthesis/modification method to avoid structural damage and to fabricate crystalline frameworks is desirable.

In the present study, we report a new strategy for the direct synthesis of magnesia-incorporated mesoporous alumina with crystalline frameworks. This strategy allows the synthesis and modification of mesoporous alumina in a one-pot process, avoids structural damage in posttreatment, and saves time and energy. We design suitable precursors for crystalline frameworks, which permits the formation of γ-Al_2O_3 frameworks at relatively low temperatures and is thus beneficial to the preservation of mesoporous structure. The resultant materials exhibit a well-defined mesoporous structure and strong basicity with excellent water-resistant ability. Moreover, the successful synthesis of mesoporous γ-Al_2O_3 functionalized with iron, chromium, and lead oxides demonstrates the generality of our strategy. These new functional materials may afford valuable candidates for catalytic and adsorptive applications.

Experimental Section

Materials Synthesis. The aluminum sources play an important role in the fabrication of mesoporous alumina, and aluminum alkoxides are widely used.[39–41] However, from the standpoint of environmental and economical considerations, inorganic aluminum salts should be more attractive candidates.[42] As a result, $Al(NO_3)_3$ was selected as starting reagent in the present study. The magnesia-incorporated mesoporous alumina was synthesized as follows. $Al(NO_3)_3 \cdot 9H_2O$ (0.1 mol) and $Mg(NO_3)_2 \cdot 6H_2O$ (0−0.05 mol) were dissolved in 20.0 g of water and then blended with 6.38 g of triblock copolymer P123 ($EO_{20}PO_{70}EO_{20}$). The resulting mixture was stirred at 40 °C for 24 h to form a clear sol. A stoichiometric amount of $NH_3 \cdot H_2O$ containing 0.3−0.4 mol of OH^- was added dropwise to the clear sol under slow stirring. The mixture was then heated to 100 °C for 24 h under static conditions to produce mesoporous alumina with transition frameworks. The solids were washed thoroughly to remove the NH_4NO_3 byproduct. The obtained materials with an Mg/Al molar ratio n ranging from 0 to 0.5 were denoted as mAl-a (if $n = 0$) or mMgAl(n)-a (if $n > 0$). Calcination of the composite was carried out in a stream of oxygen, for which the sample was heated to 500 °C at a rate of 2 °C·min^{-1} and maintained at the final temperature for 4 h, leading to the formation of γ-Al_2O_3 frameworks. The resultant materials, that is, magnesia-incorporated mesoporous γ-Al_2O_3, were denoted as mAl-γ (if $n = 0$) or mMgAl(n)-γ (if $n > 0$), where n represents the Mg/Al molar ratio. The synthesis of Fe, Cr, and Pb-functionalized mesoporous γ-Al_2O_3 is similar to that of mMgAl-γ, except that $Fe(NO_3)_3 \cdot 9H_2O$, $Cr(NO_3)_3 \cdot 9H_2O$, or $Pb(NO_3)_2$ was added instead of $Mg(NO_3)_2 \cdot 6H_2O$. The obtained materials were denoted as mFeAl(n)-γ, mCrAl(n)-γ, and mPbAl(n)-γ, where n represents the metal/Al molar ratio.

Characterization. The structure of the materials was characterized by X-ray diffraction (XRD), transmission electron microscopy (TEM), and N_2 adsorption methods. XRD patterns were recorded with a Bruker D8 Advanced diffractometer using Cu Kα radiation in the 2θ range from 0.6° to 6° or from 6° to 80° at 40 kV and 30 mA. TEM and energy-dispersive X-ray (EDX) analyses were performed on a JEM-2010 UHR electron microscope operated at 200 kV. N_2 adsorption−desorption isotherms were measured on a Micromeritics ASAP 2020 system at −196 °C and the samples were previously outgassed at 300 °C for 4 h. The Brunauer−Emmett−Teller (BET) surface area was calculated from adsorption data in the relative pressure range from 0.04 to 0.20, and the total pore volume was determined from the amount adsorbed at a relative pressure of about 0.99. The pore diameter was calculated from the desorption branch by the Barrett−Joyner−Halenda (BJH) method.

The surface and bulk element compositions of the samples were determined by X-ray photoelectron spectroscopy (XPS) and X-ray fluorescence (XRF) analyses, respectively. XPS measurement was carried out on a DTAVG Escalab Mark II XPS instrument using Mg Kα radiation. The XRF analysis was conducted on an ARL Advant' XP X-ray fluorescence spectrometer.

In a CO_2-temperature programmed desorption (CO_2-TPD) experiment, the sample was activated at 600 °C for 2 h prior to the adsorption of CO_2 at 25 °C. After the physically adsorbed CO_2 was purged at 25 °C, the sample was heated to 600 °C at the rate of 8 °C·min^{-1}, and the CO_2 liberated was detected by a mass analyzer where the mass signal of 44 was used to represent the CO_2 desorbed. The base strength (H_-) of the sample was detected by using a series of Hammett indicators. To measure the total amount of basic sites, 50 mg of sample after activation was shaken in 10 mL of aqueous HCl (0.05 M) for 24 h and the slurry was separated by a centrifuge. The remaining acid in liquid phase was titrated with aqueous NaOH (0.02 M). In a similar process, the aqueous-soluble amount of basic sites was determined. The sample (50 mg) was shaken in 10 mL of water, and the solution obtained from centrifugation of the slurry was neutralized with 10 mL of aqueous HCl (0.02 M). The remaining acid was then titrated with a standard base (aqueous NaOH, 0.01 M), and phenolphthalein was employed as the indicator.

Results

Structural Characterization of MgO-Incorporated Mesoporous γ-Al_2O_3. Figure 1A displays the low-angle XRD patterns of mesoporous γ-Al_2O_3 with and without incorporation of MgO. A single diffraction line is observed for all samples. This pattern is characteristic of a mesoporous structure with no long-range order in the pore arrangement and is similar to that observed for mesoporous aluminas obtained by hydrothermal synthesis and microwave heating.[42,43] With the increase of Mg content, the intensity of the diffraction line decreases. Figure 2A exhibits the TEM image of mMgAl(0.1)-γ sample. The presence of wormholelike pore structure is evident, which is consistent with the low-angle XRD results. Figure 3 shows the N_2 adsorption−desorption isotherms and pore size distributions of different samples. All isotherms are of classic type IV with a clear hysteresis loop, implying the mesoporosity of materials. No uptake at relative pressure (p/p_0) higher than 0.8 appears in the isotherm of mAl-γ, which corresponds to a single pore size distribution at ca. 4 nm. It is worth noting that the shape of isotherms changes obviously after introduction of Mg species. N_2 uptake at relative pressures higher than 0.8 emerges and is enhanced with increasing Mg content. Correspondingly, the bimodal pore size distributions were observed on mMgAl-γ samples. The synthesis of Mg-containing samples with bimodal pore size distributions by using single templating is noticeable. On the basis of these results, it is clear that the mesoporous structure has been successfully fabricated for mMgAl-γ samples.

As shown in Figure 1B, the sample mAl-γ displays typical diffraction lines ascribed to γ-Al_2O_3 (JCPDS 10-0425) in the wide-angle XRD pattern. The diffraction lines become slightly weaker and broader after the introduction of Mg species. It should be noted that the position of the (440) diffraction line shifts to lower diffraction angles with increasing Mg content. The lattice parameters of different samples were calculated and

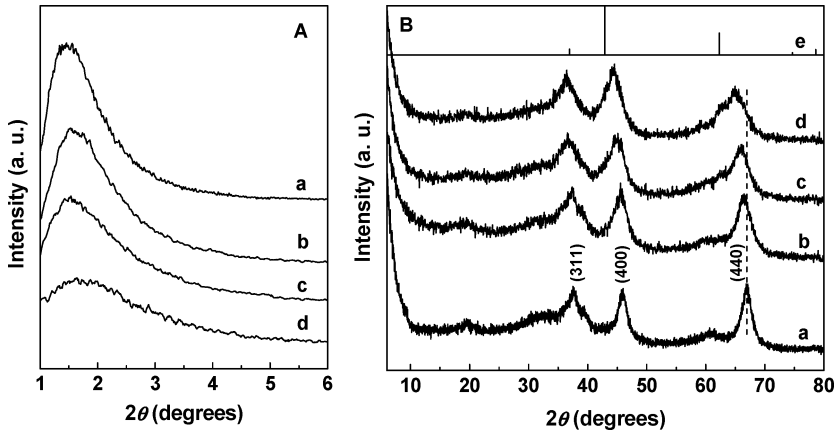

Figure 1. (A) Low-angle and (B) wide-angle XRD patterns of (a) *m*Al-γ, (b) *m*MgAl(0.1)-γ, (c) *m*MgAl(0.3)-γ, (d) *m*MgAl(0.5)-γ, and (e) MgO (JCPDS 78-0430).

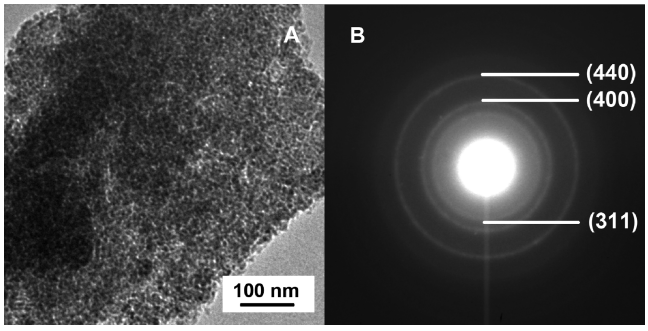

Figure 2. (A) TEM image and (B) ED pattern of *m*MgAl(0.1)-γ.

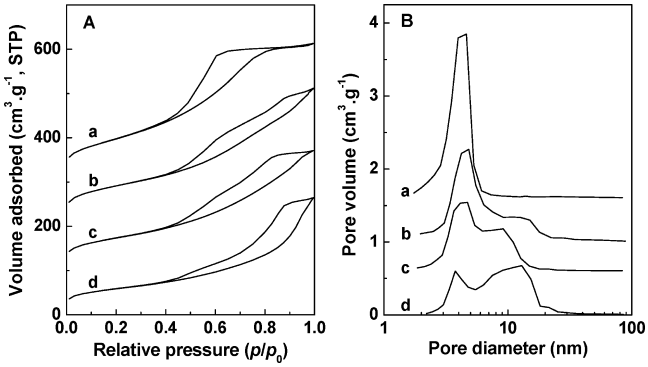

Figure 3. (A) N_2 adsorption−desorption isotherms and (B) pore size distributions of (a) *m*Al-γ, (b) *m*MgAl(0.1)-γ, (c) *m*MgAl(0.3)-γ, and (d) *m*MgAl(0.5)-γ. The ordinates are plotted offset for clarity.

are listed in Table 1. The lattice parameter of pure alumina *m*Al-γ is 0.7920 nm, while those of Mg-containing samples are obviously larger. With increasing Mg content, the lattice parameters of *m*MgAl-γ samples increase, and that of *m*MgAl(0.5)-γ can reach 0.8117 nm. Additionally, the diffraction lines at 43° and 63° attributed to MgO (JCPDS 78-0430) become visible in samples with a high Mg content (Figure 1B), indicative of the formation of crystalline MgO. Figure 2B presents the electron diffraction (ED) pattern of *m*MgAl(0.1)-γ sample. The diffraction rings assigned to (311), (400), and (440) reflections of γ-Al_2O_3 are evident, which confirms the wide-angle XRD data. By combination of the results of wide-angle XRD and ED, it is conclusive that the synthesized *m*MgAl-γ samples possess the crystalline frameworks of γ-Al_2O_3.

The successful fabrication of *m*MgAl-γ with mesoporous structure and γ-Al_2O_3 frameworks is attributed to the preparation of suitable precursors. The structural properties of these precursors are thus investigated. As shown in Figure 4A, all preassembled samples exhibit a single diffraction line, suggesting the wormhole pore structure of *m*MgAl-a sample. As compared with *m*MgAl-a, the diffraction lines in low-angle XRD patterns of *m*MgAl-γ (Figure 1A) are stronger. This means that the mesoporous structure can be well preserved during the transformation of precursors to target materials. Figure 4B presents the wide-angle XRD patterns of the precursors. The sample *m*Al-a displays the typical XRD pattern of boehmite (AlOOH, JCPDS 21-1307), which is a good precursor for γ-Al_2O_3, and the conversion of boehmite to γ-Al_2O_3 initiates at 400 °C.[44] Interestingly, the introduction of Mg species results in an obvious change of framework crystal. The diffraction lines of hydrotalcite emerge in XRD patterns of *m*MgAl-a,[45] and their intensity increases with increasing Mg content. In addition, the crystal of brucite (JCPDS 74-2220) was detected on Mg-containing samples. Despite the fact that the framework crystals of *m*MgAl-a vary with the Mg content, they can be transformed to γ-Al_2O_3 crystalline frameworks at a relatively low temperature (500 °C).

The above-mentioned results have proven the formation of crystalline frameworks and mesoporous structure of the synthesized materials. Some evidence also reveals the presence of Mg species, but the quantitative analysis and distribution behavior are scarce. Characterization of the *m*MgAl-γ samples by XRF, XPS, and EDX was thus performed. As shown in Table 1, the bulk Mg/Al ratios obtained from XRF analysis are in agreement with theoretical values, indicating that the added Mg species have been well recovered. Table 1 also displays the surface composition of samples determined by XPS. The Mg/Al ratio on the surface is nearly equal to that of bulk for *m*MgAl(0.1)-γ. With increasing Mg content, however, the surface Mg/Al ratios become smaller than that of the bulk. This suggests that the Mg species are preferentially located inside the pore channels in the samples with a high Mg content. Figure 5 depicts the EDX spectrum of the sample *m*MgAl(0.1)-γ. This local element composition analysis verifies the presence of Mg and Al in the sample. The detected Mg/Al molar ratios are similar even though several random areas are selected for EDX analysis, which implies a homogeneous distribution of Mg species on mesoporous alumina.

Basic Properties of MgO-Incorporated Mesoporous γ-Al_2O_3. The basic properties of samples were initially characterized by Hammett indicators and a basicity titration. A base strength (H_-) of less than 9.3 was determined for pure alumina *m*Al-γ. Nonetheless, the incorporation of MgO leads to an

TABLE 1: Physicochemical Characteristics of Different Samples

sample	S_{BET} ($m^2 \cdot g^{-1}$)	V_p ($cm^3 \cdot g^{-1}$)	Mg/Al atomic ratio			lattice parameter[c] (nm)
			theoretical	bulk[a]	surface[b]	
*m*Al-γ	355	0.478	0	0	0	0.7920
*m*MgAl(0.1)-γ	328	0.462	0.1	0.08	0.09	0.7956
*m*MgAl(0.3)-γ	265	0.411	0.3	0.28	0.20	0.7999
*m*MgAl(0.5)-γ	209	0.389	0.5	0.48	0.36	0.8117

[a] Measured by XRF. [b] Measured by XPS. [c] Calculated from wide-angle XRD patterns.

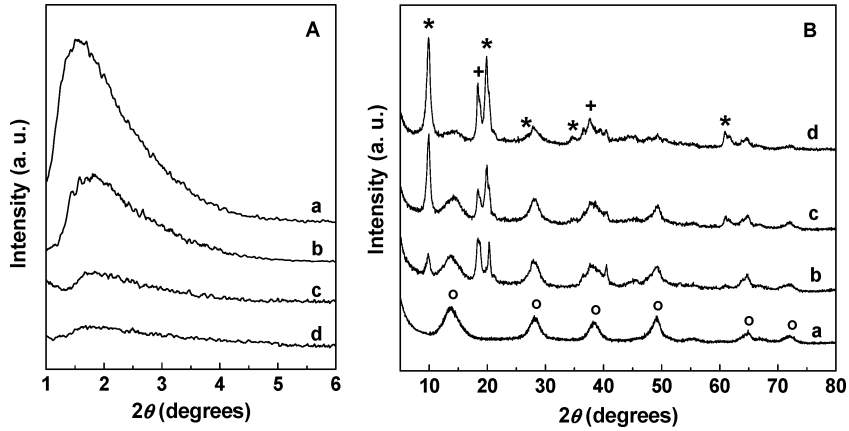

Figure 4. (A) Low-angle and (B) wide-angle XRD patterns of (a) *m*Al-a, (b) *m*MgAl(0.1)-a, (c) *m*MgAl(0.3)-a, and (d) *m*MgAl(0.5)-a. Symbols denote the crystals of (○) boehmite, (*) hydrotalcite, and (+) brucite.

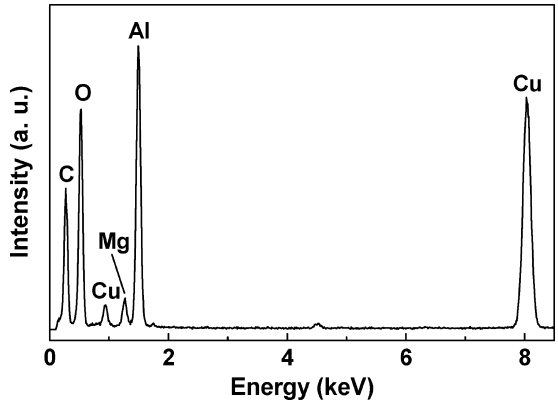

Figure 5. EDX spectrum of the *m*MgAl(0.1)-γ sample.

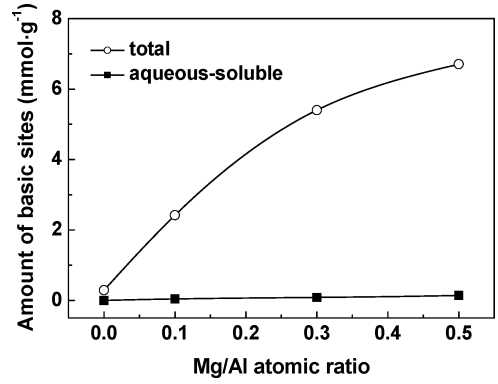

Figure 6. Total and aqueous-soluble amount of basic sites in samples with different Mg/Al atomic ratios.

obvious enhancement of base strength, and a high strength of 18.4 is detected. This indicates the generation of strongly basic sites on mesoporous alumina. The introduction of MgO also increases the number of basic sites in the composites. As can be seen from Figure 6, the total amount of basic sites in *m*Al-γ is 0.29 $mmol \cdot g^{-1}$. In contrast to *m*Al-γ, the sample *m*MgAl(0.1)-γ possesses a much higher total amount of basic sites (2.42 $mmol \cdot g^{-1}$). The total amount of basic sites keeps increasing with increasing Mg content, and that of *m*MgAl(0.5)-γ can reach 6.71 $mmol \cdot g^{-1}$. It is noteworthy that the aqueous-soluble amount of basic sites in these materials is quite tiny (less than 0.14 $mmol \cdot g^{-1}$; Figure 6), being extremely different from the total amount of basic sites. The negligible aqueous-soluble amount of basic sites implies the excellent water resistance of *m*MgAl-γ samples. This excellent water-resistant ability should result from the low solubility of the basic Mg species in water along with the interaction between the Mg species and the host. This property is helpful for expanding the application of solid bases in those processes involving water.

The results of CO_2-TPD shown in Figure 7 confirm the generation of strong basicity in *m*MgAl-γ samples. Pure mesoporous alumina (*m*Al-γ) possesses a low capacity to adsorb CO_2. Two desorption peaks at 95 and 127 °C (deconvolution results) occur in the CO_2-TPD profiles. Introduction of Mg species improves the basicity of the sample, both the amount of CO_2 desorbed and the desorption temperature increase. The broad desorption peaks centered at 224 °C [for *m*MgAl(0.3)-γ] and 262 °C [for *m*MgAl(0.5)-γ] further give evidence of the strong basicity of the Mg-containing samples. The CO_2-TPD results indicate the basicity of *m*MgAl-γ is comparable to, if not stronger than, that reported for mesoporous MgO replicated from CMK-3 carbon.[46]

Generality of Direct Synthesis Strategy. To demonstrate the generality of the present strategy, the direct synthesis of mesoporous alumina functionalized with other metal (i.e., iron, chromium, and lead) oxides was conducted. Figure 8 gives the XRD patterns of *m*FeAl(0.1)-γ, *m*CrAl(0.1)-γ, and *m*PbAl(0.1)-γ. A single diffraction line is observed in low-angle XRD patterns of these samples, which is similar to that of *m*MgAl-γ and indicates the wormholelike mesoporous structure. Wide-angle XRD patterns exhibit the diffraction lines ascribed to γ-Al_2O_3, implying that the crystalline frameworks are successfully formed. As can be seen from Figure 7B, diffraction lines

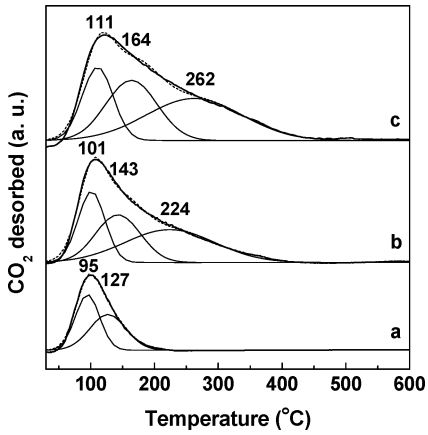

Figure 7. CO_2-TPD profiles of (a) *m*Al-γ, (b) *m*MgAl(0.3)-γ, and (c) *m*MgAl(0.5)-γ.

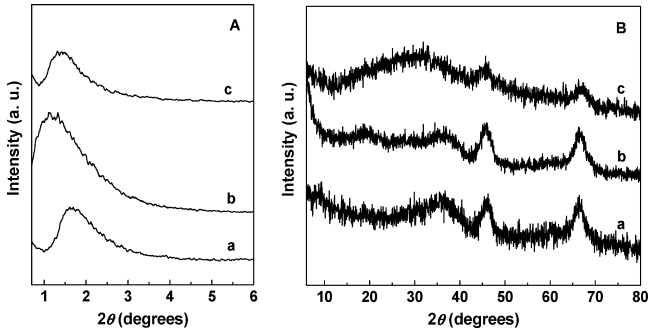

Figure 8. (A) Low-angle and (B) wide-angle XRD patterns of (a) *m*FeAl(0.1)-γ, (b) *m*CrAl(0.1)-γ, and (c) *m*PbAl(0.1)-γ.

in the XRD pattern of *m*PbAl(0.1)-γ are relatively weaker than those in other samples. Because the metal/Al molar ratio is the same for the samples, the weight percentage content of guest metal oxides is quite different. The content of Fe_2O_3, Cr_2O_3, and PbO in samples is calculated to be 14, 13, and 30 wt %, respectively. Apparently the PbO content is higher, which should be responsible for the weak γ-Al_2O_3 diffraction lines of *m*PbAl(0.1)-γ sample. In addition, a broad peak centered at about 30° was observed for the *m*PbAl(0.1)-γ sample. Although identification is difficult from this single peak, the formation of lead carbonate is proposed (JCPDS 17-0731), taking account of the interaction between PbO and atmospheric CO_2. The IR spectrum of *m*PbAl(0.1)-γ sample shows vibration bands at 1506 and 1394 cm^{-1} (data not shown), which confirms the production of carbonate.[47]

Figure 9 depicts the N_2 adsorption−desorption isotherms and pore size distributions of Fe, Cr, and Pb-containing samples. The isotherms are of type IV with little or no additional uptake at high partial pressures. Each of the isotherms has a clear hysteresis loop, which indicates the mesoporosity of the materials. All samples display narrow and uniform pore size distributions. Similar to *m*MgAl-γ, the samples *m*FeAl(0.1)-γ, *m*CrAl(0.1)-γ, and *m*PbAl(0.1)-γ have large BET surface areas (i.e., 298, 381, and 270 $m^2 \cdot g^{-1}$ respectively). It is noticeable that the surface area of *m*CrAl(0.1)-γ reaches 381 $m^2 \cdot g^{-1}$, which is even larger than that of *m*Al-γ (355 $m^2 \cdot g^{-1}$). This can be attributed to the smaller pore diameter of *m*CrAl(0.1)-γ (3.7 nm) as compared with *m*Al-γ (4.6 nm). On the basis of the foregoing results, it is clear that some metal oxides other than MgO can be incorporated into mesoporous alumina by the direct synthesis strategy. The obtained samples exhibit well-defined mesostructure, high surface areas, and γ-Al_2O_3 frameworks, which demonstrates the generality of our strategy.

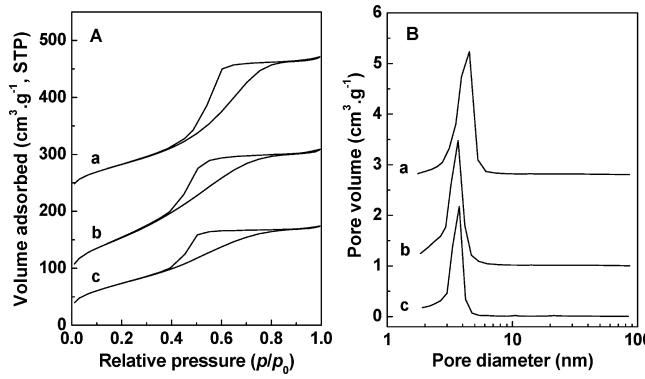

Figure 9. (A) N_2 adsorption−desorption isotherms and (B) pore size distributions of (a) *m*FeAl(0.1)-γ, (b) *m*CrAl(0.1)-γ, and (c) *m*PbAl(0.1)-γ. The ordinates are plotted offset for clarity.

Discussion

Because of the usefulness of γ-Al_2O_3, many attempts have been made to crystallize frameworks of preassembled mesoporous alumina. The crystallization of amorphous alumina to γ-Al_2O_3 typically requires temperatures higher than 700 °C, which is harmful to the mesostructure.[48] For the aim of forming crystalline frameworks at relatively low temperatures, a suitable precursor should be designed. For example, the conversion of boehmite to γ-Al_2O_3 initiates at 400 °C.[44] As described above, mesoporous alumina with boehmite frameworks is successfully synthesized. Interestingly, the addition of magnesium salt in the synthesis system leads to the formation of hydrotalcite besides boehmite, while this phenomenon is absent during the synthesis of Fe, Cr, and Pb-containing samples. The yield of hydrotalcite is fascinating, since the calcination of hydrotalcite can produce mixed oxides, which are strongly basic with high potential in many organic reactions.[49] It is known that hydrotalcite-like compounds belong to a class of anionic clay minerals. A wide variety of compounds with hydrotalcite structure can be prepared, represented by the general formula $[M^{2+}_{(1-x)}M^{3+}_x(OH)_2]A^{n-}_{x/n} \cdot mH_2O$, where $M^{2+} = Mg^{2+}$, Ni^{2+}, etc.; $M^{3+} = Al^{3+}$, Fe^{3+}, Ga^{3+}, etc.; and $A^{n-} = CO_3^{2-}$, NO_3^-, Cl^-, etc.[50] Structurally, they are formed by brucite-like sheets where isomorphous substitution of Mg^{2+} by a trivalent cation like Al^{3+} occurs.[51] Hence, brucite seems to be necessary for the formation of hydrotalcite. In the present study, the synthesis system containing nitrates of Mg and Al as well as ammonia may provide an appropriate environment for the construction of brucite, as evidenced by XRD analysis. Subsequently, the substitution of Mg^{2+} by Al^{3+} takes place and the structure of hydrotalcite is formed. After calcination at 500 °C, all samples exhibit unambiguous γ-Al_2O_3 crystalline frameworks, demonstrating that the preassembled mesoporous frameworks are suitable precursors and can be transformed to γ-Al_2O_3 at a relatively low temperature.

Differing from other mesoporous alumina samples containing metal oxides, *m*MgAl-γ samples display bimodal pore size distributions. The bimodal pore size distributions can be ascribed to the different crystalline phase of precursors. It is found that where there is a hydrotalcite phase in the precursor, a bimodal pore size distribution results. Also, the larger pores in pore size distribution curves increase with increasing hydrotalcite phase in XRD patterns. By combining the XRD and N_2 adsorption results, it should be reasonable to conclude that the smaller pores originate from the decomposition of boehmite, while the larger pores come from the conversion of hydrotalcite.

As described above, the incorporation of Mg species in mesoporous alumina results in a shift of the (440) diffraction

line to lower diffraction angles, which is also reflected quantitatively by the lattice parameters. It is known that γ-Al_2O_3 has a spinel structure, and cations can insert into the vacancies on its surface. Because the ionic radius of Mg is larger than that of Al, the insertion of Mg species leads to lattice expansion. This gives rise to a decline in the cationic deficiency of γ-Al_2O_3, thus stabilizing the structure.[52] The insertion of metal ions in vacancies and the resultant lattice expansion have also been reported on Ni-modified alumina samples.[53] It should be stated that two kinds of vacancies exist on the surface of γ-Al_2O_3, that is, tetrahedral and octahedral vacancies, and Mg^{2+} can insert into both kinds of vacancies.[54,55] In terms of previous studies,[56–58] the dispersion capacity of MgO on *m*Al-γ is estimated to be about 17 wt % theoretically, corresponding to a sample with Mg/Al atomic ratio of 0.26. Once the loading amount of MgO exceeds the dispersion capacity, crystalline MgO appears in the XRD patterns of the composites. Hence, diffraction lines attributed to MgO are detected in samples *m*MgAl(0.3)-γ and *m*MgAl(0.5)-γ. As Figure 1 presents, the diffraction lines of MgO are relatively weak. Two factors are considered to be responsible for the phenomenon. The first factor is that only part of MgO contributes to the XRD diffraction lines. As described above, only when the amount of MgO surpasses the dispersion capacity (17 wt %) does residual MgO become detectable by XRD. The second factor is that the residual MgO may exist in a microcrystalline structure, which leads to low intensity of XRD diffraction lines.[59,60]

Apart from saving time and energy, the present direct synthesis strategy plays a crucial role in the fabrication of strongly basic materials with good mesostructure. Mesoporous aluminas are less stable than their silica analogues; their mesoporous structure is easily damaged by postsynthesis modification. As a comparison, MgO-modified mesoporous γ-Al_2O_3 sample with Mg/Al molar ratio of 0.1 was thus prepared by conventional wet impregnation. The diffraction line in low-angle XRD pattern for the sample from wet impregnation is much weaker than that from direct synthesis (data not shown). Moreover, the surface area and pore volume of the impregnated sample are 239 $m^2 \cdot g^{-1}$ and 0.355 $cm^3 \cdot g^{-1}$, respectively, smaller than those of the sample from direct synthesis (surface area 328 $m^2 \cdot g^{-1}$; pore volume 0.462 $cm^3 \cdot g^{-1}$). The present strategy therefore allows the mesoporous alumina to maintain its structure, whereas wet impregnation leads to considerable structural damage.

In comparison with application of the direct synthesis method in mesoporous silicas, less attention has been given to the use of such a method in mesoporous aluminas. The synthesis of mesoporous aluminas is much more difficult to control than their silica analogues; the addition of guest species can thus disturb the synthesis system and subsequently lead to the deterioration of mesostructure. Furthermore, the frameworks of mesoporous silica are amorphous and the crystal transformation of frameworks is not needed in the synthesis process. However, crystalline frameworks (e.g., γ-type) are commonly demanded for mesoporous aluminas from the point of view of applications. In other words, the synthesis method must be delicately designed to ensure the introduction of guest species, crystal transformation of frameworks, and fabrication of mesoporous structure. These factors make it difficult to prepare functional mesoporous aluminas in a one-pot process. In the present study, we take advantage of the interaction between guest and host species and permit the formation of suitable precursors for crystalline frameworks. The γ-Al_2O_3 frameworks are thus generated at a relatively low temperature. Guest oxides are produced simultaneously during calcination and in situ coated on newly formed mesoporous γ-Al_2O_3. Accordingly, the obtained functional materials show both a well-defined mesostructure and crystalline frameworks. The successful synthesis of mesoporous γ-Al_2O_3 functionalized with various metal oxides demonstrates the generality of the present method. Our strategy may open up a route for the functionalization of mesoporous nonsiliceous materials.

Conclusions

In summary, a strongly basic material, namely, magnesia-incorporated mesoporous γ-Al_2O_3, has been successfully synthesized by a direct synthesis strategy. The present strategy performs both synthesis and modification in a one-pot process and is thus helpful for the preservation of mesoporous structure. The obtained materials exhibit strong basicity with excellent water-resistant ability, well-developed mesoporous structure, and γ-Al_2O_3 crystalline frameworks. Besides *m*MgAl-γ, some other mesoporous γ-Al_2O_3 materials functionalized with iron, chromium, and lead oxides are also prepared through our strategy. These functional materials may provide promising candidates for applications in catalysis and adsorption.

Acknowledgment. The Natural Science Foundation of Jiangsu Province Colleges (09KJB530004), the Major Basic Research Project of Natural Science Foundation of Jiangsu Province Colleges (08KJA530001), the National Science Foundation of China (20976082), and the Academic Foundation for Young Teachers in Nanjing University of Technology are acknowledged for their financial support of this research.

References and Notes

(1) Ono, Y. *J. Catal.* **2003**, *216*, 406.
(2) Seki, T.; Ikeda, S.; Onaka, M. *Microporous Mesoporous Mater.* **2006**, *96*, 121.
(3) Shanbhag, G. V.; Choi, M.; Kim, J.; Ryoo, R. *J. Catal.* **2009**, *264*, 88.
(4) Davis, M. E. *Acc. Chem. Res.* **1993**, *26*, 111.
(5) Smit, B.; Maesen, T. L. M. *Nature* **2008**, *451*, 671.
(6) Sun, L. B.; Chun, Y.; Gu, F. N.; Yue, M. B.; Yu, Q.; Wang, Y.; Zhu, J. H. *Mater. Lett.* **2007**, *61*, 2130.
(7) Sun, L. B.; Gu, F. N.; Chun, Y.; Kou, J. H.; Yang, J.; Wang, Y.; Zhu, J. H.; Zou, Z. G. *Microporous Mesoporous Mater.* **2008**, *116*, 498.
(8) Narasimharao, K.; Hartmann, M.; Thiel, H. H.; Ernst, S. *Microporous Mesoporous Mater.* **2006**, *90*, 377.
(9) Costarrosa, L.; Ruiz-Martinez, J.; Rios, R. V. R. A.; Silvestre-Albero, J.; Rojas-Cervantes, M. L.; Sepulveda-Escribano, A. *Microporous Mesoporous Mater.* **2009**, *120*, 115.
(10) Hathaway, P. E.; Davis, M. E. *J. Catal.* **1998**, *119*, 497.
(11) Baba, T.; Hikita, S.; Koide, R.; Ono, Y. *J. Chem. Soc., Faraday Trans.* **1993**, *89*, 3177.
(12) Lee, S. C.; Lee, S. W.; Kim, K. S.; Lee, T. J.; Kim, D. H.; Kim, J. C. *Catal. Today* **1998**, *44*, 253.
(13) Kresge, C. T.; Leonowicz, M. E.; Roth, W. J.; Vartuli, J. C.; Beck, J. S. *Nature* **1992**, *359*, 710.
(14) Asefa, T.; MacLachan, M. J.; Coombs, N.; Ozin, G. A. *Nature* **1999**, *402*, 867.
(15) Kim, S. S.; Zhang, W. Z.; Pinnavaia, T. J. *Science* **1998**, *282*, 1302.
(16) Mercier, L.; Pinnavaia, T. J. *Adv. Mater.* **1997**, *9*, 500.
(17) Liu, X. Y.; Tian, B. Z.; Yu, C. Z.; Gao, F.; Xie, S. H.; Tu, B.; Che, R. C.; Peng, L. M.; Zhao, D. Y. *Angew. Chem., Int. Ed.* **2002**, *41*, 3876.
(18) Wan, Y.; Zhao, D. Y. *Chem. Rev.* **2007**, *107*, 2821.
(19) De Vos, D. E.; Dams, M.; Sels, B. F.; Jacobs, P. A. *Chem. Rev.* **2002**, *102*, 3615.
(20) Davis, M. E. *Nature* **2002**, *417*, 813.
(21) Stein, A. *Adv. Mater.* **2003**, *15*, 763.
(22) Scott, B. J.; Wirnsberger, G.; Stucky, G. D. *Chem. Mater.* **2001**, *13*, 3140.
(23) Ma, X.; Wang, X.; Song, C. *J. Am. Chem. Soc.* **2009**, *131*, 5777.
(24) Xie, Y.; Sharma, K. K.; Anan, A.; Wang, G.; Biradar, A. V.; Asefa, T. *J. Catal.* **2009**, *265*, 131.

(25) Kao, H. M.; Liao, C. H.; Palani, A.; Liao, Y. C. *Microporous Mesoporous Mater.* **2008**, *113*, 212.
(26) Yan, Z.; Li, G. T.; Mu, L.; Tao, S. Y. *J. Mater. Chem.* **2006**, *18*, 1717.
(27) Weitkamp, J.; Hunger, M.; Rymsa, U. *Microporous Mesoporous Mater.* **2001**, *48*, 255.
(28) Xia, Y.; Mokaya, R. *Angew. Chem., Int. Ed.* **2003**, *42*, 2639.
(29) Wang, J.; Liu, Q. *Microporous Mesoporous Mater.* **2005**, *83*, 225.
(30) Kloetstra, K. R.; van Bekkum, H. *Stud. Surf. Sci. Catal.* **1997**, *105*, 431.
(31) Kloetstra, K. R.; van Laren, M.; van Bekkum, H. *J. Chem. Soc., Faraday Trans.* **1997**, *93*, 1211.
(32) Sun, L. B.; Gu, F. N.; Chun, Y.; Yang, J.; Wang, Y.; Zhu, J. H. *J. Phys. Chem. C* **2008**, *112*, 4978.
(33) Yamaguchi, T.; Ookawa, M. *Catal. Today* **2006**, *116*, 191.
(34) Wu, Z. Y.; Jiang, Q.; Wang, Y. M.; Wang, H. J.; Sun, L. B.; Shi, L. Y.; Xu, J. H.; Wang, Y.; Chun, Y.; Zhu, J. H. *Chem. Mater.* **2006**, *18*, 4600.
(35) Sun, L. B.; Kou, J. H.; Chun, Y.; Yang, J.; Gu, F. N.; Wang, Y.; Zhu, J. H.; Zou, Z. G. *Inorg. Chem.* **2008**, *47*, 4199.
(36) Yang, P.; Zhao, D.; Margolese, D. I.; Chmelka, B. F.; Stucky, G. D. *Nature* **1998**, *396*, 152.
(37) Yuan, Q.; Yin, A. X.; Luo, C.; Sun, L. D.; Zhang, Y. W.; Duan, W. T.; Liu, H. C.; Yan, C. H. *J. Am. Chem. Soc.* **2008**, *130*, 3465.
(38) Sun, L. B.; Yang, J.; Kou, J. H.; Gu, F. N.; Chun, Y.; Wang, Y.; Zhu, J. H.; Zou, Z. G. *Angew. Chem., Int. Ed.* **2008**, *47*, 3418.
(39) Zhang, Z.; Hicks, R. W.; Pauly, T. R.; Pinnavaia, T. J. *J. Am. Chem. Soc.* **2002**, *124*, 1592.
(40) Cejka, J. *Appl. Catal., A* **2003**, *254*, 327.
(41) Morris, S. M.; Fulvio, P. F.; Jaroniec, M. *J. Am. Chem. Soc.* **2008**, *130*, 15210.
(42) Zhang, Z.; Pinnavaia, T. J. *J. Am. Chem. Soc.* **2002**, *124*, 12294.
(43) Ren, T. Z.; Yuan, Z. Y.; Su, B. L. *Langmuir* **2004**, *20*, 1531.
(44) Kresge, C. T.; Leonowicz, M. E.; Roth, W. J; Vartuli, J. C.; Beck, J. S. *Nature* **1992**, *359*, 710.
(45) Valente, J. S.; Cantu, M. S.; Figueras, F. *Chem. Mater.* **2008**, *20*, 1230.
(46) Roggenbuck, J.; Tiemann, M. *J. Am. Chem. Soc.* **2005**, *127*, 1096.
(47) Diez, V. K.; Apesteguia, C. R.; Di Cosimo, J. I. *J. Catal.* **2006**, *240*, 235.
(48) Gonzalez-Pena, V.; Diaz, I.; Marquez-Alvarez, C.; Sastre, E.; Perez-Pariente, J. *Microporous Mesoporous Mater.* **2001**, *44*−*45*, 203.
(49) Figueras, F. *Top. Catal.* **2004**, *29*, 189.
(50) Valente, J. S.; Figueras, F.; Gravelle, M.; Kumbhar, P.; Lopez, J.; Besse, J. P. *J. Catal.* **2000**, *189*, 370.
(51) Climent, M. J.; Corma, A.; Iborra, S.; Epping, K.; Velty, A. *J. Catal.* **2004**, *225*, 316.
(52) Wang, J. A.; Morales, A.; Bokhimi, X.; Novaro, O. *Chem. Mater.* **1999**, *11*, 308.
(53) Kim, P.; Kim, Y.; Kim, H.; Song, I. K.; Yi, J. *Appl. Catal., A* **2004**, *272*, 157.
(54) Chen, Y.; Zhang, L. *Catal. Lett.* **1992**, *12*, 51.
(55) Xie, Y. C.; Tang, Y. Q. *Adv. Catal.* **1990**, *37*, 1.
(56) Sun, L. B.; Gu, F. N.; Gao, L.; Yang, J.; Kou, J. H.; Chun, Y.; Wang, Y.; Zhu, J. H.; Zou, Z. G. Nanoporous Materials, Proceedings of the 5th International Symposium, Vancouver, Canada, 2008; p 487.
(57) Zhu, J. H.; Wang, Y.; Chun, Y.; Wang, X. S. *J. Chem. Soc., Faraday Trans.* **1998**, *94*, 1163.
(58) Liu, Z.; Dong, L.; Ji, W.; Chen, Y. *J. Chem. Soc., Faraday Trans.* **1998**, *94*, 1137.
(59) Kirszensztejn, P.; Przekop, R.; Szymkowiak, A.; Mackowska, E.; Gaca, J. *Microporous Mesoporous Mater.* **2006**, *89*, 150.
(60) Gomez, M. F.; Cadus, L. E.; Abello, M. E. *Solid State Ionics* **1997**, *98*, 245.

JP907224F